

Efficient Anomaly Detection Using Self-Supervised Multi-Cue Tasks

Loïc Jézéquel, Ngoc-Son Vu, Jean Beaudet, and Aymeric Histace

Abstract—Deep anomaly detection has proven to be an efficient and robust approach in several fields. The introduction of self-supervised learning has greatly helped many methods including anomaly detection where simple geometric transformation recognition tasks are used. However these methods do not perform well on fine-grained problems since they lack finer features and are usually highly dependent on the anomaly type. In this paper, we explore each step of self-supervised anomaly detection with pretext tasks. First, we introduce novel discriminative and generative tasks which focus on different visual cues. A piece-wise jigsaw puzzle task focuses on structure cues, while a tint rotation recognition is used on each piece for colorimetry and a partial re-colorization task is performed. In order for the re-colorization task to focus more on the object rather than on the background, we propose to include the contextual color information of the image border. Then, we present a new out-of-distribution detection function and highlight its better stability compared to other out-of-distribution detection methods. Along with it, we also experiment different score fusion functions. Finally, we evaluate our method on a comprehensive anomaly detection protocol composed of object anomalies with classical object recognition, style anomalies with fine-grained classification and local anomalies with face anti-spoofing datasets. Our model can more accurately learn highly discriminative features using these self-supervised tasks. It outperforms state-of-the-art with up to 36% relative error improvement on object anomalies and 40% on face anti-spoofing problems.

Index Terms—Anomaly detection, fine grained classification, self-supervised learning, multi-task learning, one-class learning

I. INTRODUCTION

ONE of the most fundamental challenge in machine learning is detecting an observation as anomalous compared to a normal baseline. Properly solving such problem with high predictability and robustness has been essential in many fields. To mention a few, in intrusion detection [1], [2] where we wish to detect untrustworthy entries on a network, fraud detection [3], [4] where a forged item or transaction must be rejected, in medical imaging [5], [6] where abnormalities in a captured image must be located, video surveillance [7]–[9] where abnormal events are detected, in manufacturing defect detection [10], [11], and even more recently adversarial attack detection [12].

With the advent of deep learning, many tasks on image data including binary classification and anomaly detection have greatly improved. Nevertheless classical binary classification still generally lacks robustness and reliability outside its training domain. Anomaly detection tries to solve this problem by only learning the normal class boundary, rather than directly discriminating anomalies from normal samples. Any observation defined outside is then deemed as anomalous. This decision rule is especially useful when the anomaly class boundary is ill-defined or continually evolving and only few anomalous training samples are available.

The recent explosion of self supervision further improved unsupervised learning abilities and reduced the needed amount of

labeled data. It enables to discriminate anomalies from normal samples by learning to solve simple tasks such as geometric transformation classification. However, even if deep anomaly detection can achieve reasonable performance, it still suffers from limitations on more challenging problems with local and fine-grained differences between anomalies and normal samples. Moreover, these methods usually have an high inference time which often renders them unusable for real-life anomaly detection problems.

In this given context, our main contributions in this paper are the following:

- We introduce three novel specialized auxiliary tasks for Self-Supervised Learning anomaly detection. These tasks allow our model to learn richer representations which better encompass image structure (Section III-A), colorimetry (Section III-B) and texture (Section III-C). With these tasks, we also explore different OOD methods and fusion functions.
- We compare our improved method with state-of-the-art using an exhaustive protocol for anomaly detection covering object, style and local anomalies even including more challenging tasks such as face anti-spoofing.
- The proposed method obtains better overall results with up to 36% AUROC relative improvement on object anomalies and 53% on face anti-spoofing from state of the art anomaly detection methods.

This paper is an extension of the work presented in [13], where we improve the detection of fine-grained anomalies by simultaneously solving in a self-supervised fashion a high-scale geometric task and a low-scale jigsaw puzzle task. We explore here more pretext tasks, address the inference complexity issue and further improve the anomaly detection performances.

First, we give an overview of anomaly detection related work in Section II. Then we present our new pretext tasks in Section III along with the anomaly score fusion methods in Section IV. The full method is summarized in Section V. Finally we provide several experiments on the influence of our model parameters, and a comparison with state-of-the-art in Section VI.

II. RELATED WORK

A. Anomaly detection

The main goal in anomaly detection is to classify a sample as normal or anomalous. Formally, we predict $P(\mathbf{x} \in \mathcal{X}_{\text{norm}})$ for an observation \mathbf{x} and a normal (or positive) class $\mathcal{X}_{\text{norm}}$. The anomalous (or negative) class is then defined implicitly as the complementary of the normal class in image space. We can generally categorize anomalies into three families:

- 1) **Object anomaly**: any object which is not included in the positive class, e.g., a cat is an object anomaly in regards to dogs.
- 2) **Style anomaly**: observations representing the same object as the positive class but with a different style or

support, e.g., a realistic mask or a printed face represent faces but with a visible different style.

- 3) **Local anomaly**: observations representing and sharing the same style as the positive class, however a localized part of the image is different. Most of the time, these anomalies are the superposition of two generative processes, e.g., a fake nose on a real face is a local anomaly.

Usually, we assume in anomaly detection that only normal samples are available during training, meaning that most methods are part of one-class learning scheme. Traditionally, one-class Support Vector Machine [14] (**OC-SVM**) or its extension the Support Vector Data Description [15] (**SVDD**) were used for anomaly detection. The anomaly score of an observation \mathbf{x} is given by its distance to a parameterized boundary Ω . OC-SVM defines Ω as an hyper-plan separating the origin from the normal samples with the maximum margin, whereas SVDD uses an hyper-sphere containing all normal samples with the minimum radius (see Fig. 1(a,b)).

Fully-unsupervised methods which learn from a set of unlabeled data containing normal samples and anomalies can also be used. Such non-deep methods include Robust Principal Component Analysis [16] (**RPCA**) or the Isolation Forest (**IF**) algorithm [17]. Rather than modeling the normal samples, the IF algorithm tries to isolate anomalies from normal samples via successive random partitions of the feature space. If the sample can be entirely isolated (i.e. be the only point in a region) in a few partitions, then it is more likely to be anomalous (see Fig. 1(c)).

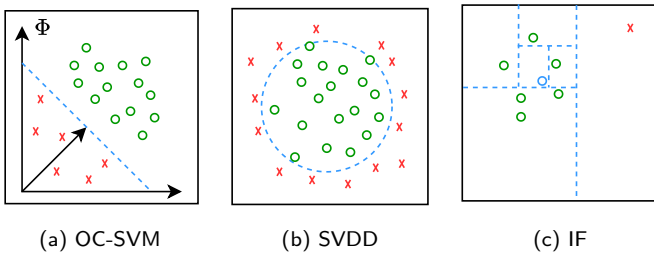


Fig. 1. Overview of classical methods where green circles are normal samples and red cross anomalies. In (a) and (b) the anomalies are not part of the training dataset. In (c) the sample on the right is predicted as anomalous since it only required a single partition, while the blue circle is deemed normal.

These classical methods have shown great success on low-dimensional data such as tabular data, however usually fail on higher dimension inputs such as images.

B. Deep anomaly detection

The introduction of neural networks as feature extractors gave birth to several hybrid methods where a pre-trained neural network is used to extract features, on which a classical algorithm such as OC-SVM or isolation forest is trained. It ultimately led to the first end-to-end anomaly detection neural network, the one-class Neural Network (**OC-NN**) [18] which integrates the OC-SVM loss in the network training. More recent methods include different dedicated approach to anomaly detection. In [19]–[21] a binary classification is used with pseudo negative images or latent vectors to represent the anomaly class. Another approach is to use the error of a generative model reconstruction [22]–[24] or the gradient of the error given that the image is normal [25]. Finally, the self-supervision framework can be used to learn normal class representations

and subsequently form an anomaly score as presented in Section II-D.

There also have been semi-supervised anomaly detection methods such as DeepSAD [26] or deviation networks [27] where we assume some of the anomalies representing a few modes are available. These methods can achieve better accuracy on borderline cases given enough diverse anomalies, which is often less manageable in practice. In particular, these two methods directly learn representations by minimizing the distance of normal sample features to an hypersphere center, while maximizing the distance to the anomalies. It follows the compactness principle, where the normal class representations variance is minimized and the inter-class representations variance is maximized.

C. Self-supervised learning

Self Supervised Learning (SSL) is a part of representation learning, where useful and general representations are learned from an unlabeled dataset. The learned features can then be used through transfer learning for a different task such as classification.

In this framework, representations are learned by solving from the data an auxiliary task \mathcal{T} , which is often unrelated to the final one. The pretext task can either be discriminative, usually resulting in a multi-class classification setting or generative where a regression loss is often utilized. Any SSL is defined by its *pretext objective loss* L and its *pretext data generation function* $G_{\mathcal{T}} : \mathcal{P}(\mathcal{X}) \mapsto \mathcal{P}(\mathcal{X} \times K)$ which yields a labeled set from an unlabeled set \mathcal{X} . In the case of discriminative tasks, it is usually done via n images transformations T_1, \dots, T_n :

$$G_{\mathcal{T}}(\{\mathbf{x}_i\}_{i \in [1, N]}) = \{(T_j(\mathbf{x}_i), j)\}_{i \in [1, N], j \in [1, n]} \quad (1)$$

where the \mathbf{x}_i are images from the unlabeled training dataset.

Therefore SSL consists of two steps: (1) generating a labeled set $\mathcal{X}_{\mathcal{T}} = G_{\mathcal{T}}(\mathcal{X})$, (2) training a classification or regression network on this generated labeled set. One of the final layers can thus be used as a feature extractor. Some commonly used tasks are: 90° rotation prediction [28], jigsaw puzzle [29], distortions [30], colorization [31], image inpainting [32] or relative patches prediction [33].

More recently, the contrastive learning framework [34] has been extensively used for self-supervised representation learning. Unlike the methods above, it does not rely on an explicit pretext task and directly formulates losses on the representations. The most effective contrastive method is instance discrimination [35], [36] where the objective is to maximize similarity between augmented versions of a same image (positive samples) while minimizing similarity with any other images (negative samples). We can still view instance discrimination as a pretext task where the pretext data generation function maps samples to the set of positive pairs and negative pairs and the objective function is to discriminate positive from negative pairs using cosine similarity in representation space.

D. SSL anomaly detection

Very recently, SSL has been adapted to the one-class anomaly detection framework. First we learn to solve an auxiliary task in a SSL fashion. Then, a measure of how well the network can solve the task on the generated dataset $G_{\mathcal{T}}(\mathcal{X})$ can be used to classify at inference time an observation \mathbf{x} as anomalous or normal. Indeed, the main assumption is that the network will perform relatively well on normal samples but will fail on

anomalies. Unlike SSL, the quantity of interest is not directly the intermediate features, but rather the final task outputs. The goals of representation learning and anomaly detection can even be opposite. Indeed, in representation learning we are interested in maximizing the performances of the representation on as many downstream tasks as possible on any other data. However in anomaly detection we want a clear discrimination through performances on normal and anomalous data.

Any SSL anomaly detection method is composed of three steps:

- 1) The **representation learning** on the normal class, which is entirely done in a self-supervised manner. In our case this is done by solving a pretext task \mathcal{T} , but other methods employ more general mechanisms such as contrastive learning.
- 2) During inference of an unseen sample \mathbf{x} , an **out-of-distribution (OOD) detection method** is applied on the generated labeled samples $G_{\mathcal{T}}(\{\mathbf{x}\})$. The main goal of OOD methods is to detect if an observation has been sampled from the same distribution as the training set. In other words, given a pre-trained model Ψ on a distribution $F_{\mathcal{X}_{\text{train}}}$, it estimates $P(\mathbf{x} \sim F_{\mathcal{X}_{\text{train}}})$. Here we assume our normal training set is close enough to the real distribution of normal samples, and since we always have access to the correct task label y , the following approximations hold:

$$s_{\text{OOD}}((\mathbf{x}, y); \Psi) \approx P(\mathbf{x} \sim F_{\mathcal{X}_{\text{train}}}) \approx P(\mathbf{x} \in \mathcal{X}_{\text{norm}}) \quad (2)$$

where $s_{\text{OOD}}((\mathbf{x}, y); \Psi)$ is the OOD score for an image \mathbf{x} with its label y given the pre-trained network Ψ .

- 3) The **fusion of the OOD scores** into a single anomaly score s_a using a fusion function M .

The full anomaly scoring function summarized in Fig. 2 is the following:

$$s_a(\mathbf{x}) = M(\{s_{\text{OOD}}((z, y); \phi \circ f) | (z, y) \in G_{\mathcal{T}}(\{\mathbf{x}\})\}) \quad (3)$$

where the network Ψ has been decomposed in an encoder ϕ and a pretext-task specific network f .

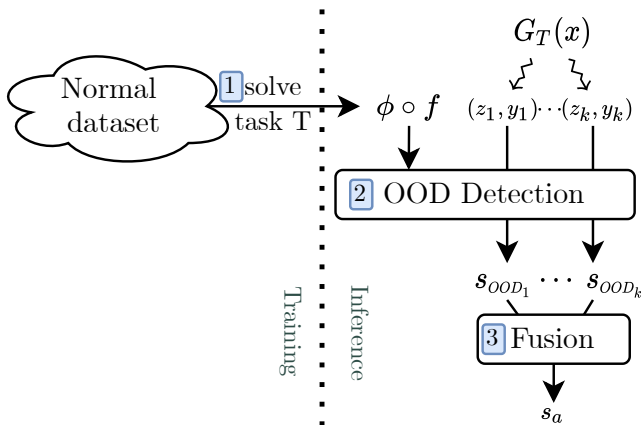


Fig. 2. The three steps of Self-Supervised Learning Anomaly Detection.

In **GeoTrans** [37], the auxiliary task is to classify which geometrical transformation has been applied to the input from a set $\{T_i\}$ of 72 random composition of translations, rotations and symmetries. At the end of training, a Dirichlet distribution

parameterized by $\tilde{\alpha}_i$ is fitted over the softmax responses of each transformation on the normal class $\mathbf{y}(T_i(\mathbf{x})) = \text{softmax}(\phi \circ f(\mathbf{x}))$; then its log-likelihood is used during inference.

$$s_a(\mathbf{x}) = \sum_{i=1}^{72} (\tilde{\alpha}_i - 1) \cdot \log \mathbf{y}(T_i(\mathbf{x})) \quad (4)$$

In **MHRot** [38], the task is to simultaneously classify vertical translation, horizontal translations and 90° rotations, each modeled by a softmax head. Accordingly, the pretext data generation function is the composition $T_{r,s,t} = \text{Rot}(r^\circ) \circ \text{HTrans}(s) \circ \text{VTrans}(t)$, where $r \in \{0, 90, 180, 270\}$, $s \in \{0, -t_x, +t_x\}$ and $t \in \{0, -t_y, +t_y\}$. During inference, the three softmax of the known transformations for each of the 36 transformation compositions are summed as anomaly score:

$$s_a(\mathbf{x}) = \sum_r \sum_s \sum_t \mathbf{y}(T_{r,s,t}(\mathbf{x}))_{r,s,t} \quad (5)$$

Another class of models, called **two-stage anomaly detectors** [39], does not use the representation learning task during inference, but rather directly apply OOD methods on the representation space [40]–[44]. For example, in **SSD** [41] the representation learning step is performed through contrastive learning, then OOD detection is applied on the representation space induced by the encoder ϕ . The training data representations are clustered around several centroids using K-means. The Mahalanobis distance is used to compute the anomaly score:

$$s_a(\mathbf{x}) = \min_m (\phi(\mathbf{x}) - \mu_m)^T \Sigma_m^{-1} (\phi(\mathbf{x}) - \mu_m) \quad (6)$$

Similarly, **DROC-contrastive** (Deep Representation One-class Classification) [39] first learn self-supervised representations from one-class data, and then build one-class classifiers on learned representations. Contrastive learning with distribution augmentation is used for the self-supervised representation learning, and a OC-SVM for the one-class classification.

An overview of our method is presented in Fig. 3. In a first stage, a jigsaw puzzle task with intra-piece tint rotation detection and a partial colorization are performed. Then in a second stage, a set of OOD scores is computed for each task and is aggregated into a single anomaly score using a fusion function. Following these two steps, we present the choice of representation learning or pretext tasks in Section III and the used OOD methods with fusion in Section IV. The jigsaw puzzle task is presented in Section III-A, the intra-piece tint rotation recognition in Section III-B, III-D and the partial colorization task in Section III-C. Finally, the choice of OOD detection function and fusion function is developed in Section IV.

III. NOVEL PRETEXT TASKS

In this section, we note $s_{\text{OOD}}((z, y); \phi \circ f)$ any out-of-distribution method producing a score from an observation z , its label y and a pre-trained network $\phi \circ f$. We gradually detail the proposed pretext tasks for anomaly detection which focus on different visual cues: structure, colorimetry and texture. The tasks of piece-wise puzzle and tint rotation are discriminative whereas the colorization task is generative.

A. Piece-wise puzzle task

The puzzle task has often been successfully used as a pretext task for representation learning [29], [45]. First an image is

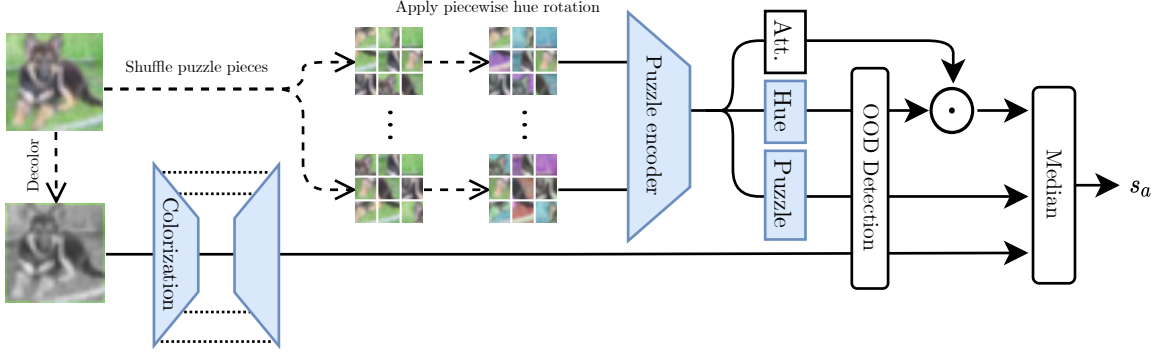


Fig. 3. Method overview.

separated into $n = n_w \times n_h$ pieces, with some margin between them and a random offset. Then given the reconstructed image with the shuffled pieces, we wish to predict which permutation has been applied. It is therefore formulated as a classification task where the prediction label corresponds to the index of the permutation among the $n!$ total possibilities. When the number of pieces becomes too large, the full task is not conceivable and we only learn to classify k randomly sampled permutations ($k \ll n$). This formulation of the jigsaw puzzle task, used in our previous work [13] along with geometrical transformation recognition, enables our model to learn low-scale fine features. In the next sections, we call this formulation the partial puzzle task.

However, this formulation presents many limitations. First, the quality of our representation highly depends on the chosen permutations. Indeed if the sampled permutations are too hard (e.g. swapping two corners) or too easy, the learned representations will suffer. Moreover from an anomaly detection perspective, we will equally penalize all predicted permutations where at least one piece is misplaced.

We thus propose an improved piece-wise puzzle task where rather than predicting the permutation index, we predict the original position of each piece. By assuming each piece is independent, we can now cover all the permutations with only n^2 outputs, where we previously needed $n!$. The task is learned using classical multi-variable classification with several cross-entropies on every possible permutations:

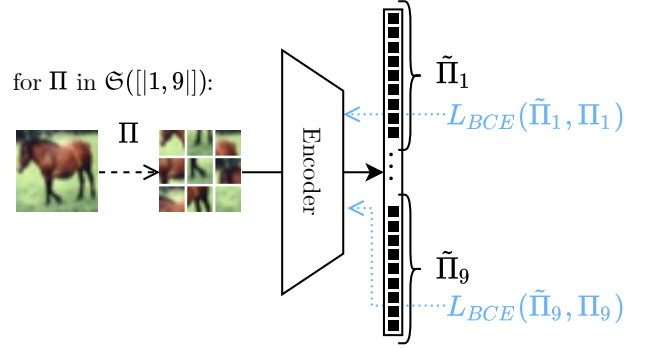
$$L_{\text{puzzle}}(I) = \frac{1}{n} \sum_{i=1}^n \log(\tilde{\Pi}_i \Pi_i) \quad (7)$$

where Π_j is the new position of the j^{th} piece and $\tilde{\Pi}_j = \text{softmax}(\phi \circ f(I)_j)$ is the prediction vector for the j^{th} piece. The full task is presented in Fig. 4. In practice, we sample during every training epoch a random subset of k' permutations for each normal image. In order to have most of the permutations in the training set, we define

$$k' = \frac{n!}{N_{\text{train}} \cdot ep} \quad (8)$$

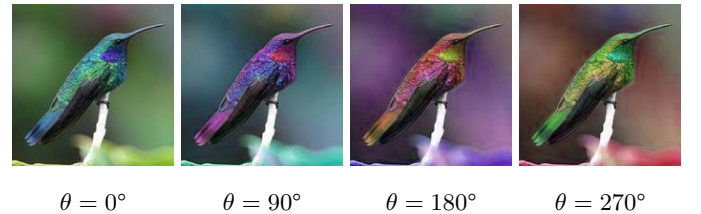
where N_{train} is the size of the training set and ep the number of training epochs. During inference we can compute for a single observation a tensor of OOD scores $(S)_{i \in [1, n_h], j \in [1, n_w], \kappa \in [1, k]}$.

In general, with this new piece-wise puzzle task lower anomaly detection errors can be reached while keeping the same inference complexity as the partial puzzle task (see results in Fig. 10).

Fig. 4. Piece-wise puzzle task for 3×3 pieces.

B. Tint rotation task

We also include tasks which are more focused on the normal class colorimetry. In this regard, we introduce a novel tint rotation recognition task. Given an RGB image \mathbf{x} and a transformation γ where $\gamma(\mathbf{x}, \theta)$ adds an offset θ to the hue channel (in HSV space) of \mathbf{x} ; we try to predict the distribution of Θ from $\gamma(\mathbf{x}, \Theta)$. For practical reasons, we limit the possible tint rotation angles to c distributed angles and our task becomes to predict $\Theta | \gamma(\mathbf{x}, \theta) \sim \text{Cat}(\{k \cdot \frac{360}{c}\}_{k \in [0, c]})$. We note that contrary to the geometrical rotation recognition task where a number of angles different than four would leave visual artifacts, we do not have any limitation on c .

Fig. 5. Tint rotation task for $c = 4$.

Desaturated areas of the object have to be ignored since any rotation of tint would be undetectable, producing high anomaly scores. Therefore, instead of working on the angle distribution we directly use the expected L_1 error in RGB space between the original image and the corrected one. The new anomaly score is:

$$s_a(\gamma(\mathbf{x}, \theta)) = \mathbb{E}_{\Theta|\gamma(\mathbf{x}, \theta)} \left[1 - \frac{\|\mathbf{x} - \gamma(\mathbf{x}, \theta - \Theta)\|_1}{W \times H \times 255} \right] \quad (9)$$

where $W \times H$ is the dimension of the image. By taking a pixel by pixel RGB error, only large areas of colorful pixels will impact the anomaly score.

By introducing this task we force our encoder to fully represent the normal class colorimetry, which the puzzle task could potentially ignore in case of salient geometrical features.

C. Partial colorization task

We now introduce a novel generative pretext task for anomaly detection which is highly texture oriented. In the colorization task [31], [46], [47], the main objective is to predict the (A, B) color channels from the luminance channel L of an image in LAB space.

One big challenge with this task is to colorize the background since it can vary a lot inside the training normal set. The re-colorization will be naturally poorer for unseen background during inference of new observations. Our decision here is that the object itself should have more impact on anomaly detection than the background, making our anomaly detector more object-oriented than scene-oriented. To make the background re-colorization easier, we augment the available inputs with the color values of the image inside a border of size b . Our partial colorization task consists in predicting (A, B) from the image $I_{\text{part}} = (L, A_{\Omega_b}, B_{\Omega_b})$ where $S_{\Omega_b, i, j} = (1 - \mathbb{1}\{i \in [b, H - b], j \in [b, W - b]\})S_{i, j}$.

Typically, colorization is often dealt through regression [46] where $\mathbb{E}[(A_{i, j}, B_{i, j})|L]$ is directly estimated for each pixel (i, j) . However using this approach in anomaly detection pretext task would introduce numerous issues:

- 1) Our normal class can potentially be multi-modal, which a regression network can not model and will end up predicting the mean of all modes.
- 2) Even if one of the object mode is correctly predicted, any error function will yield high values if the mode of the current observation is different.

Therefore, different to existing regression methods, we estimate the posterior density $p(A_{i, j}, B_{i, j}|I_{\text{part}})$ of each pixel. For density estimation, we explore two different ideas: (1) quantize the colors into a low-range discrete variable and perform multi-class classification; (2) parameterize the density with a gaussian mixture model and perform maximum likelihood estimation.

1) *Color bin classification*: Our first approach for color density estimation is via bin classification. By quantizing each color value into K bins and assuming the two colors planes to be independent, we can define the resulting categorical variables by $2K$ probabilities: $P(A_{i, j} = 1), \dots, P(A_{i, j} = K), P(B_{i, j} = 1), \dots, P(B_{i, j} = K)$. We thus estimate a map y of dimension $H \times W \times 2K$, where

$$y_{i, j, 2k} = P(A_{i, j} = k|I_{\text{part}}) \quad (10)$$

$$y_{i, j, 2k+1} = P(B_{i, j} = k|I_{\text{part}}) \quad (11)$$

Taken from the label smoothing idea [48], a gaussian smoothing is applied to the output distributions in order to propagate our model confidence to neighbor color bins. Indeed we do not want to entirely penalize close color bins. As such the final estimated density $\hat{P}(A_{i, j}|I_{\text{part}})$ for a network ϕ is

$$\hat{P}(A_{i, j} = k|I_{\text{part}}) = (\text{softmax}(\phi(I_{\text{part}})_{i, j}) \star G_{\sigma})_k \quad (12)$$

where G_{σ} is the gaussian kernel of standard deviation σ .

2) *Gaussian Mixture Model MLE*: Our second approach is to parameterize the densities with Gaussian Mixture Models [49]. Accordingly, we have for each pixel a sum of K gaussian densities:

$$p(A_{i, j}, B_{i, j}|I_{\text{part}}) = \sum_{k=1}^K \pi_{i, j}^{(k)} \mathcal{N}(A_{i, j}, B_{i, j}; \mu_{i, j}^{(k)}, \Sigma_{i, j}^{(k)}) \quad (13)$$

where $\pi_{i, j}^{(k)} \in \mathbb{R}$ is the prior probability of the k^{th} cluster, $\mu_{i, j}^{(k)} \in \mathbb{R}^2$ is the mean color of the k^{th} cluster and $\Sigma_{i, j}^{(k)} \in \mathbb{R}^{2 \times 2}$ is the covariance color matrix of the k^{th} cluster.

Rather than predicting the full 2×2 matrix $\Sigma_{i, j}^{(k)}$, we only predict the three free parameters σ . We can then reconstruct the positive definite covariance matrix using Cholesky decomposition [50]:

$$\Sigma_{i, j}^{(k)} = L(l)\text{Diag}(\exp(d))L(l)^T \quad (14)$$

where $\sigma = (d \in \mathbb{R}^2, l \in \mathbb{R})$, $L(l) = \begin{pmatrix} 1 & 0 \\ l & 1 \end{pmatrix}$. This decomposition ensures strictly positive eigen values from the exponential and a semi-positive matrix from the Cholesky decomposition. All the possible covariance matrices are thus parameterized by σ . It also introduces better numerical stability for determinant computation:

$$\log |\Sigma| = \log |\text{Diag}(\exp(d))| = \sum_i d_i \quad (15)$$

To train this model, we could use as the loss function the log-likelihood which is considering all pixels are independent:

$$L(\mu, \Sigma|A, B) = \sum_{i, j} \log \left(\sum_{k=1}^K \pi_{i, j}^{(k)} \mathcal{N}(A_{i, j}, B_{i, j}; \mu_{i, j}^{(k)}, \Sigma_{i, j}^{(k)}) \right) \quad (16)$$

However this function turns out to be very hard to directly optimize for each pixel and does not lead to any meaningful colorization. We use instead the classical Expectation Maximization algorithm [51]: which translates our case into

- 1) **Compute Mahalanobis distances**:

$$\Delta_{i, j}^{(k)} = \left(I_{i, j} - \mu_{i, j}^{(k)} \right)^T \Sigma_{i, j}^{(k)-1} \left(I_{i, j} - \mu_{i, j}^{(k)} \right) \quad (17)$$

- 2) **Compute posterior cluster probabilities**:

$$\gamma_{i, j}(k) = \frac{\pi_{i, j}^{(k)} \exp \left(-\frac{1}{2} \left(\sum_l d_l^{(k)} + \Delta_{i, j}^{(k)} \right) \right)}{\sum_{\kappa=1}^K \pi_{i, j}^{(\kappa)} \exp \left(-\frac{1}{2} \left(\sum_l d_l^{(\kappa)} + \Delta_{i, j}^{(\kappa)} \right) \right)} \quad (18)$$

- 3) **Fix the $\gamma_{i, j}(k)$ and minimize loss**:

$$L(\pi, \mu, \Sigma|I) = \sum_{i, j} \sum_{k=1}^K \gamma_{i, j}(k) \left(\Delta_{i, j}^{(k)} + \sum_l d_l^{(k)} - \log \pi_{i, j}^{(k)} \right) \quad (19)$$

In order to choose the number of gaussians K , we apply beforehand a K-means color clusterization [52] on the cropped down-sampled images of the normal class. Then by using the elbow method, we can find the optimal K inside $\llbracket 1, 10 \rrbracket$.

The GMM approach has several advantages over the bin classification: (i) its density support is not bounded, and is continuous thus not needing any gaussian smoothing (ii) it can fully model the dependence between the color channels with the full covariance matrix (iii) it can reach the same quality of colorization with fewer parameters. The quality of colorization is here measured using the mean pixel color likelihood.

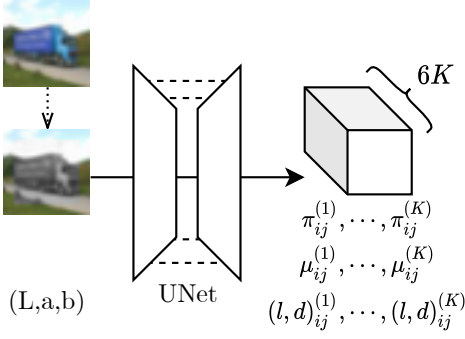


Fig. 6. Scheme of the partial colorization with GMM estimation and a UNet network (Section VI-B).

D. Intra-piece tasks

On top of the piece-wise puzzle task, we choose to add pretext sub-tasks inside each puzzle piece. Given an intra-piece task \mathcal{T}_{piece} and an image composed of n pieces images I_1, \dots, I_n , we first sample a random augmented piece using the pretext data generation function on each piece $(I_i^{aug}, y_i) \sim G_{\mathcal{T}_{piece}}(\{I_i\})$. Then our network tries to solve simultaneously the puzzle task and the intra-piece tasks by minimizing the loss

$$L(I) = L_{\text{puzzle}}(I) + \frac{1}{n} \sum_{i,j} L_{\text{intra-piece}}(I_{i,j}) \quad (20)$$

where L_{puzzle} is the piece-wise puzzle loss defined in Equation 7 and $L_{\text{intra-piece}}$ is the loss of the intra-piece task. A summary of the intra-piece task model is given in Fig. 7.

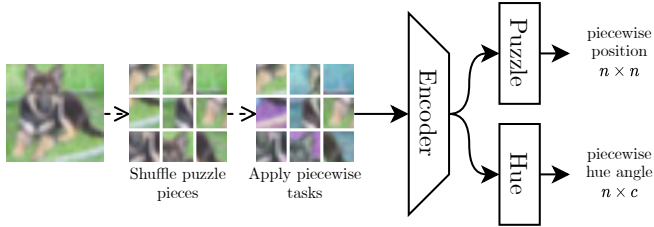


Fig. 7. Example of intra-piece tasks with hue rotation detection with c possible rotations.

By adding these intra-piece tasks, we essentially test n new tasks during inference without increasing the number of forward pass in our encoder. The only cost is the additional specialized dense layer for the pretext task. Each intra-piece task will allow our network to focus on specific image patches.

One issue with this method is that we can potentially mix object pieces and background pieces. Since the background is only loosely related to the object, solving tasks on background pieces would not make sense and would enable the model to generalize on image distribution far from the normal class. As a result, we introduce a weight map for each piece learned during training where higher weights are given for pieces covering the object. We could see this map as a rough segmentation of the normal object in the image. These are computed in a similar fashion as visual attention mechanism, which have previously been used for learning weight maps for each pixels [53], [54].

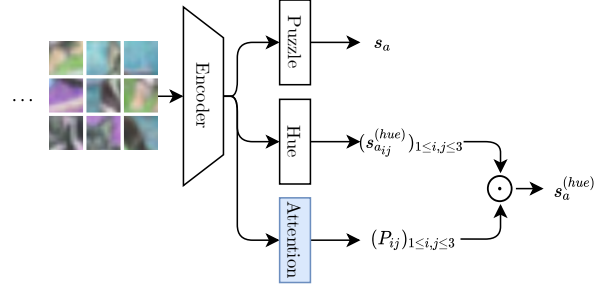


Fig. 8. Intra-piece tasks with attention.

First, we compute from the encoder representation z a weight map $(P_{ij})_{0 \leq i+j \leq n}$, which we normalize using the L_1 norm of the sigmoid:

$$P'_{ij} = \frac{\sigma(P_{ij})}{\|P\|_1} \quad (21)$$

This normalization function produces smoother maps than the classical softmax activation, preventing degenerate maps where only the center piece has a positive weight. To further prevent these cases, we include an additional term to the loss encouraging spread matrices:

$$\mu = \sum_{i,j} P_{ij} \begin{pmatrix} i \\ j \end{pmatrix} \quad (22)$$

$$L_{\text{density}}(P) = \sum_{i,j} \left\| \begin{pmatrix} i \\ j \end{pmatrix} - \mu \right\|_2 P_{ij} \quad (23)$$

These weights are then taken into account in the loss function

$$L = L_{\text{puzzle}}(I) + L_{\text{density}}(P') + \sum_{i,j} P'_{ij} \cdot L_{\text{intra-piece task}}(I_{i,j}) \quad (24)$$

and the computation of the anomaly score

$$s_a(\mathbf{x}) = M(\{s_{OOD}((z, y); \phi \circ f) | (z, y) \in G_{\mathcal{T}}(\{\mathbf{x}\})\}) \quad (25)$$

We can see in Table VIII that the attention mechanism increases the AUC on several datasets.

IV. OOD METHODS AND FUSION

We try different out-of-distribution methods for each pretext task. In the case of a self-supervised classification task, the easiest OOD function is the likelihood of the label given that the image is normal, which we call the "softmax truth":

$$s_{OOD}((z, y); \phi \circ f) = p(y|z, z \in \mathcal{X}_{\text{train}}) \approx \text{softmax}(\phi \circ f(z))_y \quad (26)$$

One of the main issues with the softmax truth is that we only take into account one component of the softmax vector. For easy tasks, we usually have a high probability on the correct class, however for harder, multi-issue task, we can have several typical highly activated classes for the normal class. As such, another idea is to look instead at the likelihood of the raw score vector given the label and that the image is normal:

$$s_{OOD}((z, y); \phi \circ f) = p(\phi \circ f(z) | y, z \in \mathcal{X}_{\text{train}}) \quad (27)$$

The distribution of the normal class raw score vectors given the label is estimated after convergence of the network weights from the partitioned training dataset $\{(z, y) | (z, y) \in \mathcal{X}_{\text{train}}, y = l\}_l$.

For a given classification problem with C classes and a training set $\mathcal{X}_{\text{norm}}$, we estimate the mean scores μ_c and covariance matrices Σ_c for each class c :

$$\mathcal{Z}_c = \{z | (z, y) \in G\mathcal{T}(\mathcal{X}_{\text{norm}}) \text{ and } y = c\} \quad (28)$$

$$\mu_c = \frac{1}{|\mathcal{Z}_c|} \sum_{z \in \mathcal{Z}_c} \phi \circ f(z) \quad (29)$$

$$\Sigma_c = \frac{1}{|\mathcal{Z}_c|} \sum_{z \in \mathcal{Z}_c} (\phi \circ f(z) - \mu_c)^2 \quad (30)$$

The OOD score is approximated by the Mahalanobis distance [55] with the mode corresponding to the truth label:

$$s_{\text{OOD}}((z, y); \phi \circ f) \approx (\phi \circ f(z) - \mu_y)^T \Sigma_y^{-1} (\phi \circ f(z) - \mu_y) \quad (31)$$

We also explore different fusion functions to combine all the OOD scores into a single anomaly score. We used previously the mean, but observed heavy biases from outlier OOD scores (very easy sub-task or harder sub-task). We tried different order statistics including the median and the 25th percentile and compare the results in Table VI.

V. FULL METHOD OVERVIEW

This section summarizes our full method. We first train independently one network on the partial re-colorization task and a second one on the piece-wise puzzle task with intra-piece hue rotation detection task. The re-colorization task is modeled with *GMM*, and we include the *attention mechanism* for the intra-piece task. To detect if an observation \mathbf{x} is an anomaly, we produce the OOD scores of the re-colorization and the k sampled permutations along with hue rotation tasks. The chosen OOD function for every task is the *label likelihood*. All of these scores are then combined into a single anomaly score using the *median*. The complete model is given in Fig. 3.

VI. RESULTS

A. Evaluation protocol

Our evaluation protocol is made of three types of anomaly detection challenges. First, we want to detect object anomalies on general coarse object recognition datasets. The one-vs-all protocol is used, where we consider one class of a multi-classification dataset as the normal class. All the other classes are then considered as anomalous, and we can obtain a set of runs for each possible normal class. The final reported result is the mean of all runs.

However, even though such datasets are easier to acquire and result in a highly multi-modal anomaly class, they have become far from real anomaly detection applications and might not be enough to fully evaluate anomaly detection methods. Thus we include a second evaluation group where we try to detect style anomalies using fine-grained classification datasets. Fine-grained datasets have been introduced to tackle the recognition of classes, usually part of a same category, with slight differences. We use here the one-vs-all protocol as well.

Finally, we include a real anomaly detection problem which incorporates object anomalies, style anomalies and local anomalies. In particular we choose a dataset from face anti-spoofing (FAS), where the goal is to discriminate real faces from fake representations of someone's face. Due to the constantly evolving frauds and high variability, anomaly detection seems a very appealing solution to this problem.

We use the following datasets:

(i) For **object anomalies**:

- **F-MNIST** [56]: has been introduced as a harder version of MNIST with 10 different classes of fashion items. All images are grayscale meaning no color information can be used to discriminate anomalies.
- **CIFAR-10** [57]: object recognition dataset composed of 10 wide classes with 6000 images per class.
- **CIFAR-100** [57]: extended version of CIFAR-10 with 100 classes each containing 600 images.

(ii) For **style anomalies**:

- **Caltech-UCSD Birds 200** [58]: fine-grained classification dataset of 200 birds species with approximately 30 images per class.
- **FounderType-200** [59]: font recognition dataset containing 200 fonts with 6700 images per class. It has been introduced for novelty detection and even though these images lie on a low dimensional manifold compared to natural images, they still provide insight into how well the model can capture small shape hints.

(iii) For the **face presentation attack detection**, we use the **WMCA** dataset [60] which contains more than 1900 short videos of real faces and presentation attacks. It contains several modalities such as infra-red or depth, but here we only use RGB. There are 72 real identities along with several types of attacks: paper print, screen replay, masks and partial attacks where only a localized area of the face is fake. The masks are composed of paper masks, rigid mask and flexible masks. An example of each type of attack is given in Fig. 9.

TABLE I
SUMMARY OF EVALUATION DATASETS.

	Dataset	Anomaly type		
		Object	Style	Local
Obj.classif	F-MNIST	✓	✗	✗
	CIFAR-10	✓	✗	✗
	CIFAR-100	✓	✗	✗
Fine-grained	Caltech-Birds	✓	✓	✗
	FounderType	✗	✓	✗
FAS	WMCA	✓	✓	✓

In all evaluations, the metric used is the area under the ROC curve (**AUROC**) or the error 1-AUROC, averaged over all possible normal classes in the case of one-vs-all datasets. We additionally include for anti-spoofing datasets metrics more adapted to biometric presentation attack detection:

- The equal error rate (**EER** [61]), which is the location in the ROC curve where the false reject rate (or Bona-fide Presentation Classification Error Rate BPCER) is equal to the false acceptance rate (or Attack Presentation Classification Error Rate APCER).
- The Attack Presentation Classification Error Rate for the Bona-fide Presentation Classification Error Rate fixed at 5% (**APCER@5%BPCER** [61]).

B. Implementation details

For the piece-wise puzzle task, we use a margin of half the size of the pieces and find best results with $k = 18$. Generally we use $n_w = n_h = 3$ pieces for most datasets, except face anti-spoofing where $n_w = 3$ and $n_h = 4$. We observe better results with more vertical pieces on faces, since they are always upright and need finer vertical analysis. For the tint rotation recognition we use $c = 4$ and for the re-colorization task, we use a contextual border of two pixels.

TABLE II

COMPARISON WITH THE STATE-OF-THE-ART AUROC OVER SEVERAL DATASETS, UNDERLINE INDICATES BEST RESULT, BOLD INDICATES BEST ONE-CLASS LEARNING RESULT. ONLY ONE-CLASS METHODS IN THE FIRST BLOCK HAVE NOT BEEN EVALUATED (RESULTS ARE FROM [39], [62], [63]). DROC-CONTRASTIVE [39] COMBINES DIFFERENT TECHNIQUES INTO TWO SEQUENTIAL TRAININGS: CONTRASTIVE REPRESENTATION LEARNING, DISTRIBUTION AUGMENTATION AND OC-SVM.

	Model	CIFAR-10	CIFAR-100	F-MNIST	CUB-200	FounderType	WMCA
Supervised	16-4 WideResNet [64]	99.3	96.3	99.2	-	-	82.4
	Deep-SAD (75%) [26]	<u>92.5</u>	88.7	<u>98.1</u>	73.6	<u>99.8</u>	83.2
Semi-Supervised	Deep-SAD (25%)	90.8	87.9	95.4	70.9	99.4	79.8
	Deep-SAD (10%)	86.0	<u>89.1</u>	88.2	66.1	98.0	72.6
One-class	ADGAN [62]	62.4	54.7	88.4	-	-	-
	GANomaly [23]	69.5	56.5	80.9	-	-	-
	ARNet [63]	86.6	78.8	93.9	-	-	-
	DROC-contrastive [39]	<u>92.5</u>	<u>86.5</u>	<u>94.8</u>	-	-	-
	OCSVM [14]	58.5	-	74.2	76.3	-	-
	IF [17]	73.4	-	84.0	74.2	-	-
	OC-CNN [20]	66.5	-	75.4	-	-	-
	PIAD [24]	79.9	78.8	94.3	63.5	90.8	76.4
	GeoTrans [37]	85.4	84.7	92.6	66.6	92.3	79.8
	MHRot [38]	89.5	83.6	92.5	77.6	96.7	81.3
	PuzzleGeom [13]	88.2	85.8	92.8	<u>83.2</u>	96.9	85.6
	Ours	<u>92.5</u>	<u>88.2</u>	93.7	<u>83.2</u>	<u>97.4</u>	<u>91.4</u>

TABLE III

DETAILED COMPARISON WITH ONE-CLASS STATE-OF-THE-ART AUROC ON CIFAR-10 DATASET.

Model	Airplane	Automobile	Bird	Cat	Deer	Dog	Frog	Horse	Ship	Truck	Avg
VAE [65]	70.0	38.6	67.9	53.5	74.8	52.3	68.7	49.3	69.6	38.6	58.3
OCSVM [14]	63.0	44.0	64.9	48.7	73.5	50.0	72.5	53.3	64.9	50.8	58.5
AnoGAN [22]	67.1	54.7	52.9	54.5	65.1	60.3	58.5	62.5	75.8	66.5	61.8
PixelCNN [66]	53.1	99.5	47.6	51.7	73.9	54.2	59.2	78.9	34.0	66.2	61.8
Deep-SVDD [67]	61.7	65.9	50.8	59.1	60.9	65.7	67.7	67.3	75.9	73.1	64.8
OCGAN [68]	75.7	53.1	64.0	62.0	72.3	62.0	72.3	57.5	82.0	55.4	65.6
Puzzle-AE [69]	78.9	78.0	69.9	54.8	75.4	66.0	74.7	73.3	83.3	69.9	72.4
DROCC [21]	81.7	76.7	66.7	67.1	73.6	74.4	74.4	71.4	80.0	76.2	74.2
AnoNAGN [70]	96.2	63.8	72.5	64.3	87.3	63.8	88.3	58.4	93.5	64.5	75.01
GeoTrans [37]	74.7	95.7	78.1	72.4	87.8	87.8	83.4	95.5	93.3	91.3	86.0
PuzzleGeom [13]	75.1	96.3	84.8	74.2	91.1	89.9	88.7	95.5	94.7	91.9	88.2
SSD [41]	82.7	98.5	84.2	84.5	84.8	90.9	91.7	95.2	92.9	94.4	90.0
Ours	85.9	97.9	88.7	81.2	95.4	94.2	92.1	96.9	96.5	95.4	<u>92.5</u>

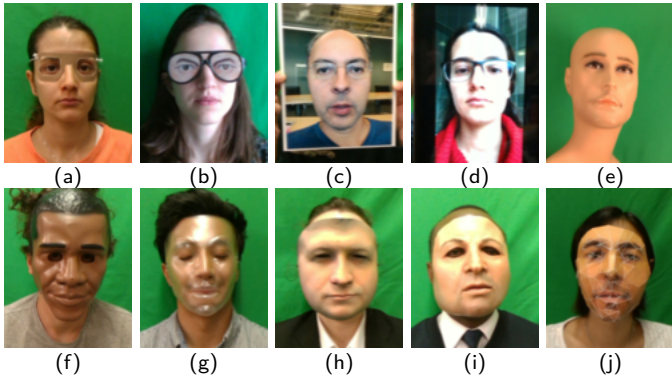


Fig. 9. Types of spoof attacks in WMCA dataset: 347 bonafide, 75 glasses (a)(b), 200 print (c), 348 replay (d), 122 fake head (e), 137 rigid mask (f)(g)(h), 379 flexible mask (i), 71 paper mask (j).

Regarding network architecture, we use a 16-4 WideResNet [64] ($\approx 10M$ parameters with a depth of 16) for the feature extractor network ϕ , along with three dense layers respectively

of size n^2 for the piece-wise puzzle task, size $n \cdot c$ for the tint rotation task and size n for the attention. Each of these dense layers have a dropout rate of 0.3 [71]. As for the re-colorization task, we use a UNet network [72]. It was originally introduced for image segmentation, using a down-sample / up-sample strategy reintroducing the intermediate maps at each step of the down-sample branch into the up-sample branch. It is in fact generally well suited for any prediction task where the output is aligned with the input pixels (in our case a vector of GMM parameters for each pixel). Training is performed under SGD optimizer with Nesterov momentum [73], using a batch size of 32 and a cosine annealing learning rate scheduler [74].

C. Comparison to the state-of-the-art

A comparison of our method with other state-of-the-art (SOTA) anomaly detection models is performed on all three protocols. We choose to include three families of SOTA methods: *one-class learning* methods which only learn using the normal class, *semi-supervised learning* methods where a small set of anomalies is used during training and *supervised learning*. The considered one-class methods can be categorized into

(1) reconstruction error-based methods with **ADGAN** [62], **GANomaly** [23] and **PIAD** [24], (2) hybrid methods with **OCSVM** [14], **IF** [17], **OC-CNN** [20], (3) pretext task-based methods with **ARNet** [63], **GeoTrans** [37], **MHRot** [38] and **PuzzleGeom** [13] and (4) two-stage anomaly detection using contrastive learning with **SSD** [41] and **DROC-contrastive** [39]. **GeoTrans** uses various geometrical transformations as SSL pretext task, **MHRot** adds on top 90° rotations and our previous model **PuzzleGeom** [13] includes a basic jigsaw puzzle task. Regarding semi-supervised methods, we evaluate **DeepSAD** [26] trained on the same normal samples but with three different ratio of the anomaly sub-classes: 10%, 25% and 75%. For the fully supervised baseline we simply use the same backbone as our one-class method (the **16-4 WideResNet**) extended with a dense layer representing the two normal and anomaly classes. It is important to note that its training is performed with classical binary cross-entropy loss on the normal/anomaly label, without any class balancing mechanism.

The experiment results are displayed in Table II and a detailed evaluation on the CIFAR-10 dataset is included in Table III. We note that for the sake of fair comparison in the same conditions, we re-evaluate most methods ourselves using existing implementations.

Our method maintains among the best accuracies on coarse object anomaly detection, even on a more challenging datasets such as CIFAR-100. It improves upon PuzzleGeom, and closes the gap toward semi-supervised performances with a small AUC difference of 0.5% on CIFAR-100. It also keeps competitive performances on fine-grained anomaly detection problems producing close results from our PuzzleGeom model. We also show that our method greatly improves anti-spoofing detection performances on WMCA. It even outperforms the supervised model and semi-supervised anomaly detection methods which have access up to 75% of the anomalous data.

In general we can notice that hybrid methods, although efficient for smaller problems, do not extend well to high-dimensional data. The evaluated reconstruction-based methods also tend to fall behind pretext-task oriented models. On the other hand, two-stage contrastive methods produce very competitive performances, as seen with DROC-contrastive. This model combines different techniques including contrastive representation learning, distribution augmentation and OC-SVM. It performs slightly better than ours on the F-MNIST dataset and reach the same AUC on CIFAR-10 but on the more challenging one, CIFAR-100, we obtained a gain of nearly 2%. Moreover, we note that distribution augmentation and OC-SVM could also be used on the concatenation of our learned representations, reaching better accuracy.

Overall, our model keeps a good balance between coarse object anomaly detection and finer style anomaly detection, and even outperforms semi-supervised anomaly detection methods on CUB-200 and WMCA. It achieves a relative error improvement of 36% on CIFAR-10 and 40% on WMCA compared to PuzzleGeom.

Lastly, we compare in Table IV our method with the two second best self-supervised methods MHRot and PuzzleGeom on WMCA. Using our method the APCER@5%BPCER drops from 33.8% to 27.3%, this also shows promising usage of anomaly detection methods in fraud detection.

TABLE IV
AUROC, EER AND APCER AT 5% BPCER ON WMCA DATASET,
BEST RESULT IS IN BOLD.

Models	AUROC	EER	APCER (5%BPCER)
MHRot [38]	81.3	23.9	72.6%
PuzzleGeom [13]	85.6	19.7	33.8%
Ours	91.4	16.1	27.3%

VII. PARAMETER STUDY

In this section, we evaluate the parametrization of pretext tasks in Section VII-A, VII-B, VII-C, the choice of OOD function in Section VII-D and perform an ablation study in Section VII-E.

A. Puzzle task complexity

We start by comparing in Fig. 10 the two approaches on the CIFAR-10 dataset for the jigsaw puzzle task introduced in Section III-A. The piece-wise puzzle task greatly improves performances for all CIFAR-10 classes even though the same permutations are tested during inference. Moreover, we confirm that the partial puzzle task is more sensitive to the choice of k , since its representation quality also depends on this factor. We choose to fix $k = 18$ as a good compromise between complexity of inference and accuracy.

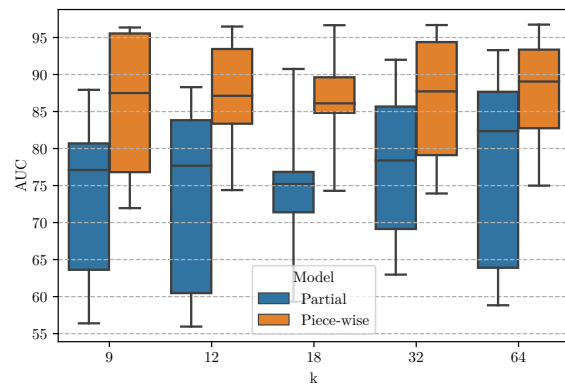


Fig. 10. Comparison of AUC with different number of tested permutations k for 3x3 partial and piece-wise puzzle on CIFAR-10 dataset.

The influence of the number of puzzle pieces n_w and n_h for $k \in \{9, 18\}$ is reported in Fig. 11 on CIFAR-10. We can see that for both $k = 9$ and $k = 18$, the best value for general one-vs-all problem is $n_w = n_h = 3$.

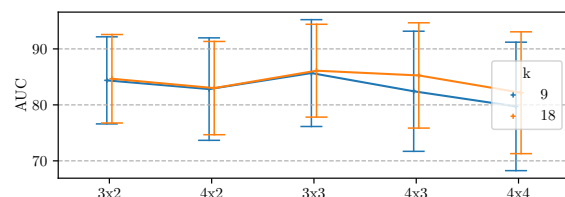


Fig. 11. Comparison of number of piece on CIFAR-10 dataset.

B. Tint rotation task complexity

We measure the AUC of the isolated tint rotation task for different number of tint rotations c on the CIFAR-10 dataset in Fig. 12. The best value of c across several normal classes is 4.

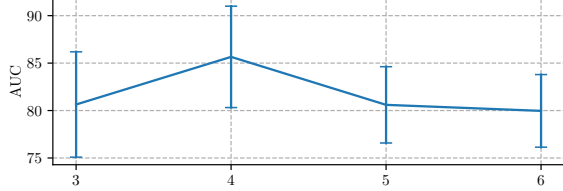


Fig. 12. Comparison of AUC with different number of tint rotation c on CIFAR-10 dataset.

C. Colorization task parametrization

The two colorization parametrizations using Gaussian Mixture Model and bin classification are compared on the normal class full colorization task. Our evaluation metric is directly the likelihood of the colorization, which is respectively for classification and GMM

$$\mathcal{L}(A, B) = \prod_{i,j} \text{softmax}(\phi(I)_{ij})_{\lfloor \frac{A_{ij}}{K} \rfloor} \cdot \text{softmax}(\phi(I)_{ij})_{\lfloor \frac{B_{ij}}{K} \rfloor} \quad (32)$$

and

$$\mathcal{L}(A, B) = \prod_{i,j} \sum_{k=1}^K \pi_{ij}^{(k)} \mathcal{N}(A_{ij}, B_{ij}; \mu_{ij}^{(k)}, \Sigma_{ij}^{(k)}) \quad (33)$$

Overall, we can reach higher likelihoods with GMM than bin classification. Moreover, a better separation of the different modes can be achieved using GMM, where bin classification usually mixes the different modes and produces dull colors (see Fig. 13).

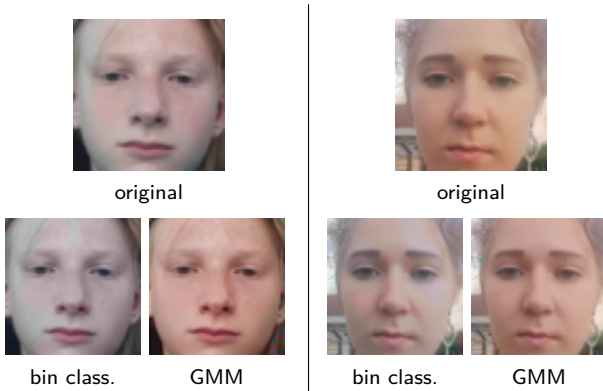


Fig. 13. Colorization comparison on faces. The first image row displays the original images, while the second represents the re-colorization where each pixel color has been sampled from the predicted distribution. As we can see, the bin classification approach produces dull colors and mixes the skin color modes, producing grayish colors.

D. Choice of OOD and fusion functions

To evaluate the effect of Mahalanobis distance as an anomaly score, we compare it with the softmax truth and its improved

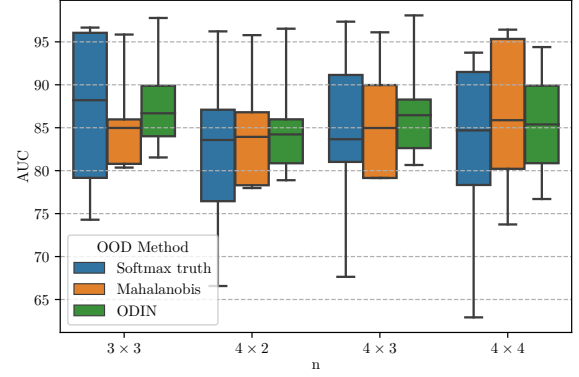


Fig. 14. Comparison of OOD methods AUC with different number of pieces n for $k = 18$ on CIFAR-10 dataset.

TABLE V
COMPARISON OF AUC WITH DIFFERENT OOD METHODS FOR THE PUZZLE TASK WITH $k = 9$ ON CIFAR-10 DATASET.

n	OOD Method	μ_{AUC}	\max_{AUC}	\min_{AUC}
3×3	Softmax truth	86.39	96.35	71.95
	Mahalanobis	83.44	95.30	80.60
4×2	Softmax truth	82.82	96.11	65.49
	Mahalanobis	83.21	95.74	80.10
4×3	Softmax truth	84.13	96.34	66.57
	Mahalanobis	84.41	96.08	81.22
4×4	Softmax truth	80.61	93.48	61.87
	Mahalanobis	86.58	96.29	80.00

form, the ODIN method [75] which adds temperature scaling during training, and the following input pre-processing:

$$\tilde{\mathbf{x}} = \mathbf{x} - \varepsilon \text{sign}(-\nabla_{\mathbf{x}} \log \text{softmax}(\mathbf{x}; T)) \quad (34)$$

The results are presented in Fig. 14 for different number of puzzle pieces n and $k = 18$ permutations tested. We notice that the AUC increases with the number of pieces when using the Mahalanobis distance, whereas it decreases with the softmax truth. In addition, the AUC of the most difficult class is always higher when using the Mahalanobis distance. This shows that despite a lower average anomaly detection performance, it has less variance in its predictions and provides more robust OOD scores to different normal classes. Even though the ODIN method provides sensible improvement for more than 3×3 pieces, it greatly increases computational complexity during training and inference. In our tests, we observe an inference time increase of more than three times with the ODIN method.

Finally, we evaluate the choice of different fusion functions on the WMCA dataset in Table VI. The evaluated fusion functions are simple order statistics commonly found among ensemble learning decision fusion strategies. We observe overall better performances regarding AUC and APCER with the median fusion function.

E. Ablation study

We evaluate the impact of each pretext task on the final anomaly detection AUROC. In Table VII, we compare on CIFAR-10 the basic partial puzzle model with the addition of the piece-wise puzzle task, colorization task, intra-piece tint rotation detection task with and without the attention map.

TABLE VI
COMPARISON OF AUC AND APCER@5%BPCER WITH DIFFERENT
FUSION FUNCTIONS FOR THE PUZZLE TASK ON WMCA DATASET.

Function	AUC	APCER (5%BPCER)
Mean	90.12 ± 0.42	30.3
25 th percentile	91.63 ± 0.50	29.2
Median	91.41 ± 0.45	27.3

While the piece-wise puzzle and colorization give our model great discrimination power with an AUC of 89.12, the intra-piece task with attention further refines our model.

TABLE VII
ABLATION STUDY OF EACH COMPONENT ON CIFAR-10 USING THE
AUROC.

Ablation Settings				AUC
Piece-wise	Colorization	Intra-piece tint	Attention	
✗	✗	✗	✗	75.44
✓	✗	✗	✗	86.97
✓	✓	✗	✗	89.12
✓	✓	✓	✗	90.94
✓	✓	✓	✓	92.48

We also investigate on more datasets how the addition of attention in the intra-piece task improves anomaly detection in Table VIII. By including attention weights for each piece, we can further improve the mean AUC on all datasets, although marginally increasing the prediction variances on different normal classes.

TABLE VIII
ABLATION STUDY OF THE INTRA-PIECE TASK ATTENTION USING THE
AUROC.

Att.	AUC		
	CIFAR10	CIFAR100	WMCA
✗	90.94 ± 0.51	88.06 ± 0.84	90.29 ± 0.34
✓	92.48 ± 0.52	88.21 ± 0.83	91.43 ± 0.35

VIII. CONCLUSION AND FUTURE WORK

We explore in this paper more efficient pretext tasks and show that a combination of a colorization and a puzzle task with intra-piece hue rotation subtasks provides the best anomaly detection performances. We also show the importance of different out-of-distribution functions along with their fusion functions. Finally, we provide a more comprehensive evaluation protocol than previously used datasets in the anomaly detection literature. It presents more challenging datasets and covers object, style and local anomalies. Our method outperforms state-of-the-art, including a semi-supervised method, on most of the fine-grained datasets.

For future work we could explore other generative pretext tasks such as image reconstruction. As in the colorization task, only a part of the image mostly covering the normal object would be destroyed. Moreover we could reframe our method into a two-stage anomaly detection. In a first step, representations would be learned solving our pretext re-colorization, jigsaw puzzle and intra-piece tint rotation detection tasks. Then we could separately train a OC-SVM on the concatenation of representations from the puzzle and colorization encoder.

REFERENCES

- [1] D. Kwon, H. Kim, J. Kim, S. C. Suh, I. Kim, and K. J. Kim, "A survey of deep learning-based network anomaly detection," *Cluster Computing*, vol. 22, no. Suppl 1, pp. 949–961, 2019.
- [2] J. Jabez and B. Muthukumar, "Intrusion Detection System (IDS): Anomaly Detection Using Outlier Detection Approach," *Procedia Computer Science*, vol. 48, pp. 338–346, 12 2015.
- [3] Z. Zhang, X. Zhou, X. Zhang, L. Wang, and P. Wang, "A model based on convolutional neural network for online transaction fraud detection," *Security and Communication Networks*, vol. 2018, pp. 1–9, 08 2018.
- [4] V. Ceronmani Sharmila, K. K. R., S. R., S. D., and H. R., "Credit Card Fraud Detection Using Anomaly Techniques," in *1st International Conference on Innovations in Information and Communication Technology (ICIICT)*, 04 2019, pp. 1–6.
- [5] N. Kumar and S. P. Awate, "Semi-supervised robust mixture models in RKHS for abnormality detection in medical images," *IEEE Trans. Image Process.*, vol. 29, pp. 4772–4787.
- [6] A. S. Lundervold and A. Lundervold, "An overview of deep learning in medical imaging focusing on mri," *Zeitschrift für Medizinische Physik*, vol. 29, no. 2, pp. 102 – 127, 2019, special Issue: Deep Learning in Medical Physics.
- [7] H. Lv, C. Zhou, Z. Cui, C. Xu, Y. Li, and J. Yang, "Localizing anomalies from weakly-labeled videos," *IEEE Trans. Image Process.*, vol. 30, pp. 4505–4515.
- [8] R. Leyva, V. Sanchez, and C. Li, "Video anomaly detection with compact feature sets for online performance," *IEEE Trans. Image Process.*, vol. 26, no. 7, pp. 3463–3478.
- [9] W. Sultani, C. Chen, and M. Shah, "Real-World Anomaly Detection in Surveillance Videos," in *IEEE/CVF Conference on Computer Vision and Pattern Recognition*, 06 2018, pp. 6479–6488.
- [10] Z. Zeng, B. Liu, J. Fu, and H. Chao, "Reference-based defect detection network," *IEEE Trans. Image Process.*, vol. 30, pp. 6637–6647.
- [11] Q. Zou, Z. Zhang, Q. Li, X. Qi, Q. Wang, and S. Wang, "Deepcrack: Learning hierarchical convolutional features for crack detection," *IEEE Trans. Image Process.*, vol. 28, no. 3, pp. 1498–1512.
- [12] A. Paudice, L. Muñoz-González, A. György, and E. C. Lupu, "Detection of adversarial training examples in poisoning attacks through anomaly detection," *CoRR*, vol. abs/1802.03041, 2018.
- [13] L. Jezequel, N. Vu, J. Beaudet, and A. Histace, "Fine-grained anomaly detection via multi-task self-supervision," in *IEEE International Conference on Advanced Video and Signal Based Surveillance*, 2021, to appear.
- [14] B. Schölkopf, R. Williamson, A. Smola, J. Shawe-Taylor, and J. Platt, "Support vector method for novelty detection," in *Proceedings of the 12th International Conference on Neural Information Processing Systems*, ser. NIPS'99. Cambridge, MA, USA: MIT Press, 1999, p. 582–588.
- [15] D. M. Tax and R. P. Duin, "Support Vector Data Description," *Machine Learning*, vol. 54, no. 1, pp. 45–66, 01 2004.
- [16] E. J. Candès, X. Li, Y. Ma, and J. Wright, "Robust principal component analysis?" *J. ACM*, vol. 58, no. 3, 06 2011.
- [17] F. T. Liu, K. Ting, and Z.-H. Zhou, "Isolation forest," in *Eighth IEEE International Conference on Data Mining*, 01 2009, pp. 413 – 422.
- [18] R. Chalapathy, A. K. Menon, and S. Chawla, "Anomaly detection using one-class neural networks," *CoRR*, vol. abs/1802.06360, 2018.
- [19] P. C. Ngo, A. A. Winarto, C. K. L. Kou, S. Park, F. Akram, and H. K. Lee, "Fence GAN: Towards Better Anomaly Detection," in *IEEE 31st International Conference on Tools with Artificial Intelligence (ICTAI)*, 11 2019, pp. 141–148.
- [20] P. Oza and V. M. Patel, "One-Class Convolutional Neural Network," *IEEE Signal Processing Letters*, vol. 26, no. 2, pp. 277–281, 02 2019.
- [21] S. Goyal, A. Raghunathan, M. Jain, H. V. Simhadri, and P. Jain, "Drocc: Deep robust one-class classification," in *International Conference on Machine Learning*, 2020.
- [22] T. Schlegl, P. Seeböck, S. M. Waldstein, U. Schmidt-Erfurth, and G. Langs, "Unsupervised anomaly detection with generative adversarial networks to guide marker discovery," in *International conference on information processing in medical imaging*. Springer, 2017, pp. 146–157.

- [23] S. Akcay, A. Atapour-Abarghouei, and T. P. Breckon, "Ganomaly: Semi-supervised anomaly detection via adversarial training," in *Asian Conference on Computer Vision*. Springer, 2018, pp. 622–637.
- [24] N. Tuluptceva, B. Bakker, I. Fedulova, and A. Konushin, "Perceptual Image Anomaly Detection," in *Pattern Recognition*, ser. Lecture Notes in Computer Science, S. Palaiahnakote, G. Sanniti di Baja, L. Wang, and W. Q. Yan, Eds. Springer International Publishing, 2020, pp. 164–178.
- [25] G. Kwon, M. Prabhushankar, D. Temel, and G. AlRegib, "Back-propagated Gradient Representations for Anomaly Detection," in *Computer Vision – ECCV*, 2020, pp. 206–226.
- [26] L. Ruff, R. A. Vandermeulen, N. Görnitz, A. Binder, E. Müller, K.-R. Müller, and M. Kloft, "Deep semi-supervised anomaly detection," in *International Conference on Learning Representations*, 2020.
- [27] G. Pang, C. Shen, and A. van den Hengel, "Deep anomaly detection with deviation networks," in *Proceedings of the 25th ACM SIGKDD International Conference on Knowledge Discovery & Data Mining, KDD, Anchorage, AK, USA*, 2019, pp. 353–362.
- [28] S. Gidaris, P. Singh, and N. Komodakis, "Unsupervised representation learning by predicting image rotations," in *6th International Conference on Learning Representations, Vancouver, BC, Canada*, 2018.
- [29] M. Noroozi and P. Favaro, "Unsupervised learning of visual representations by solving jigsaw puzzles," in *Computer Vision – ECCV*, 2016, pp. 69–84.
- [30] A. Dosovitskiy, P. Fischer, J. T. Springenberg, M. A. Riedmiller, and T. Brox, "Discriminative unsupervised feature learning with exemplar convolutional neural networks," *IEEE Trans. Pattern Anal. Mach. Intell.*, vol. 38, no. 9, pp. 1734–1747, 2016.
- [31] R. Zhang, P. Isola, and A. A. Efros, "Colorful image colorization," in *Computer Vision - ECCV - 14th European Conference, Amsterdam, The Netherlands*, vol. 9907, 2016, pp. 649–666.
- [32] D. Pathak, P. Krähenbühl, J. Donahue, T. Darrell, and A. A. Efros, "Context encoders: Feature learning by inpainting," in *IEEE Conference on Computer Vision and Pattern Recognition, Las Vegas, NV, USA*, 2016, pp. 2536–2544.
- [33] C. Doersch, A. Gupta, and A. A. Efros, "Unsupervised visual representation learning by context prediction," in *2015 IEEE International Conference on Computer Vision, ICCV 2015, Santiago, Chile, December 7-13, 2015*. IEEE Computer Society, 2015, pp. 1422–1430.
- [34] P. Le-Khac, G. Healy, and A. Smeaton, "Contrastive Representation Learning: A Framework and Review," *IEEE Access*, vol. 8, pp. 193 907–193 934, 01 2020.
- [35] T. Chen, S. Kornblith, M. Norouzi, and G. E. Hinton, "A simple framework for contrastive learning of visual representations," in *Proceedings of the 37th International Conference on Machine Learning*, vol. 119, 2020, pp. 1597–1607.
- [36] J.-B. Grill, F. Strub, F. Altché, C. Tallec, P. Richemond, E. Buchatskaya, C. Doersch, B. Avila Pires, Z. Guo, M. Gheshlaghi Azar, B. Piot, k. kavukcuoglu, R. Munos, and M. Valko, "Bootstrap your own latent - a new approach to self-supervised learning," in *Advances in Neural Information Processing Systems*, vol. 33, 2020, pp. 21 271–21 284.
- [37] I. Golan and R. El-Yaniv, "Deep anomaly detection using geometric transformations," in *Advances in Neural Information Processing Systems 31*, S. Bengio, H. Wallach, H. Larochelle, K. Grauman, N. Cesa-Bianchi, and R. Garnett, Eds. Curran Associates, Inc., 2018, pp. 9758–9769.
- [38] D. Hendrycks, M. Mazeika, S. Kadavath, and D. Song, "Using self-supervised learning can improve model robustness and uncertainty," in *Advances in Neural Information Processing Systems 32, Vancouver, BC, Canada*, 2019, pp. 15 637–15 648.
- [39] K. Sohn, C. Li, J. Yoon, M. Jin, and T. Pfister, "Learning and evaluating representations for deep one-class classification," in *9th International Conference on Learning Representations, Austria*.
- [40] J. Tack, S. Mo, J. Jeong, and J. Shin, "CSI: novelty detection via contrastive learning on distributionally shifted instances," *Advances in Neural Information Processing Systems 33: Annual Conference on Neural Information Processing Systems 2020, NeurIPS 2020, virtual*, 2020.
- [41] V. Sehwal, M. Chiang, and P. Mittal, "SSD: A unified framework for self-supervised outlier detection," in *9th International Conference on Learning Representations, Austria*, 2021.
- [42] T. Reiss and Y. Hoshen, "Mean-shifted contrastive loss for anomaly detection," vol. abs/2106.03844.
- [43] C. Li, K. Sohn, J. Yoon, and T. Pfister, "Cutpaste: Self-supervised learning for anomaly detection and localization," in *IEEE Conference on Computer Vision and Pattern Recognition, CVPR 2021, virtual, June 19-25, 2021*. Computer Vision Foundation / IEEE, pp. 9664–9674.
- [44] S. Han, H. Song, S. Lee, S. Park, and M. Cha, "Elsa: Energy-based learning for semi-supervised anomaly detection," vol. abs/2103.15296.
- [45] F. M. Carlucci, A. D'Innocente, S. Bucci, B. Caputo, and T. Tommasi, "Domain generalization by solving jigsaw puzzles," in *IEEE Conference on Computer Vision and Pattern Recognition, Long Beach, CA, USA*, 2019, pp. 2229–2238.
- [46] S. Iizuka, E. Simo-Serra, and H. Ishikawa, "Let there be color! joint end-to-end learning of global and local image priors for automatic image colorization with simultaneous classification," *ACM Trans. Graph.*, vol. 35, no. 4, jul 2016.
- [47] J.-W. Su, H.-K. Chu, and J.-B. Huang, "Instance-Aware Image Colorization," in *IEEE/CVF Conference on Computer Vision and Pattern Recognition*, 06 2020, pp. 7965–7974.
- [48] R. Müller, S. Kornblith, and G. E. Hinton, "When does label smoothing help?" in *Advances in Neural Information Processing Systems 32, Vancouver, BC, Canada*, 2019, pp. 4696–4705.
- [49] D. A. Reynolds, "Gaussian mixture models," in *Encyclopedia of Biometrics*, S. Z. Li and A. K. Jain, Eds. Springer US, 2009, pp. 659–663.
- [50] N. Higham, "Cholesky Factorization," *Wiley Interdisciplinary Reviews: Computational Statistics*, vol. 1, pp. 251–254, 09 2009.
- [51] T. Moon, "The expectation-maximization algorithm," *IEEE Signal Processing Magazine*, vol. 13, no. 6, pp. 47–60, 11 1996.
- [52] X. Jin and J. Han, "K-means clustering," in *Encyclopedia of Machine Learning*, C. Sammut and G. I. Webb, Eds. Springer, 2010, pp. 563–564.
- [53] K. Xu, J. Ba, R. Kiros, K. Cho, A. C. Courville, R. Salakhutdinov, R. S. Zemel, and Y. Bengio, "Show, attend and tell: Neural image caption generation with visual attention," in *Proceedings of the 32nd International Conference on Machine Learning, Lille, France*, vol. 37, 2015, pp. 2048–2057.
- [54] W. Wang and J. Shen, "Deep visual attention prediction," *IEEE Trans. Image Process.*, vol. 27, no. 5, pp. 2368–2378, 2018.
- [55] G. J. McLachlan, "Mahalanobis distance," *Resonance*, vol. 4, no. 6, pp. 20–26, 06 1999.
- [56] H. Xiao, K. Rasul, and R. Vollgraf, "Fashion-mnist: a novel image dataset for benchmarking machine learning algorithms," *CoRR*, vol. abs/1708.07747, 2017.
- [57] A. Krizhevsky, "Learning multiple layers of features from tiny images," 2009.
- [58] P. Welinder, S. Branson, T. Mita, C. Wah, F. Schroff, S. Belongie, and P. Perona, "Caltech-UCSD Birds 200," California Institute of Technology, Tech. Rep. CNS-TR-2010-001, 2010.
- [59] J. Liu, Z. Lian, Y. Wang, and J. Xiao, "Incremental kernel null space discriminant analysis for novelty detection," in *IEEE Conference on Computer Vision and Pattern Recognition*, 07 2017, pp. 4123–4131.
- [60] A. George, Z. Mostaani, D. Geissenbuhler, O. Nikisins, A. Anjos, and S. Marcel, "Biometric Face Presentation Attack Detection With Multi-Channel Convolutional Neural Network," *IEEE Transactions on Information Forensics and Security*, vol. 15, pp. 42–55, 2020.
- [61] I. Chingovska, A. Mohammadi, A. Anjos, and S. Marcel, "Evaluation methodologies for biometric presentation attack detection," in *Handbook of Biometric Anti-Spoofing - Presentation Attack Detection, Second Edition*, ser. Advances in Computer Vision and Pattern Recognition, S. Marcel, M. S. Nixon, J. Fierrez, and N. W. D. Evans, Eds. Springer, 2019, pp. 457–480.
- [62] L. Deecke, R. Vandermeulen, L. Ruff, S. Mandt, and M. Kloft, "Image Anomaly Detection with Generative Adversarial Networks," in *Machine Learning and Knowledge Discovery in*

- Databases*, ser. Lecture Notes in Computer Science, M. Berlingerio, F. Bonchi, T. Gärtner, N. Hurley, and G. Ifrim, Eds. Springer International Publishing, 2019, pp. 3–17.
- [63] Y. Fei, C. Huang, C. Jinkun, M. Li, Y. Zhang, and C. Lu, “Attribute Restoration Framework for Anomaly Detection,” *IEEE Transactions on Multimedia*, pp. 1–1, 2020.
 - [64] S. Zagoruyko and N. Komodakis, “Wide residual networks,” in *Proceedings of the British Machine Vision Conference, York, UK*, 2016.
 - [65] D. P. Kingma and M. Welling, “Auto-encoding variational bayes,” in *2nd International Conference on Learning Representations, Banff, AB, Canada*, 2014.
 - [66] A. Van den Oord, N. Kalchbrenner, L. Espeholt, O. Vinyals, A. Graves *et al.*, “Conditional image generation with pixelcnn decoders,” in *Advances in neural information processing systems*, 2016, pp. 4790–4798.
 - [67] L. Ruff, R. A. Vandermeulen, N. Görnitz, L. Deecke, S. A. Siddiqui, A. Binder, E. Müller, and M. Kloft, “Deep one-class classification,” in *Proceedings of the 35th International Conference on Machine Learning*, vol. 80, 2018, pp. 4393–4402.
 - [68] P. Perera, R. Nallapati, and B. Xiang, “Ocgan: One-class novelty detection using gans with constrained latent representations,” in *Proceedings of the IEEE Conference on Computer Vision and Pattern Recognition*, 2019, pp. 2898–2906.
 - [69] M. Salehi, A. Eftekhari, N. Sadjadi, M. H. Rohban, and H. R. Rabiee, “Puzzle-ae: Novelty detection in images through solving puzzles,” *CoRR*, vol. abs/2008.12959, 2020.
 - [70] C. Chen, W. Yuan, Y. Xie, Y. Qu, Y. Tao, H. Song, and L. Ma, “Novelty detection via non-adversarial generative network,” *CoRR*, vol. abs/2002.00522, 2020.
 - [71] N. Srivastava, G. E. Hinton, A. Krizhevsky, I. Sutskever, and R. Salakhutdinov, “Dropout: a simple way to prevent neural networks from overfitting,” *J. Mach. Learn. Res.*, vol. 15, no. 1, pp. 1929–1958, 2014.
 - [72] O. Ronneberger, P. Fischer, and T. Brox, “U-net: Convolutional networks for biomedical image segmentation,” in *Medical Image Computing and Computer-Assisted Intervention, Munich, Germany*, vol. 9351, 2015, pp. 234–241.
 - [73] I. Sutskever, J. Martens, G. Dahl, and G. Hinton, “On the importance of initialization and momentum in deep learning,” in *Proceedings of the 30th International Conference on Machine Learning*, vol. 28, no. 3, 2013, pp. 1139–1147.
 - [74] I. Loshchilov and F. Hutter, “SGDR: stochastic gradient descent with warm restarts,” in *5th International Conference on Learning Representations, Toulon, France*, 2017.
 - [75] S. Liang, Y. Li, and R. Srikant, “Enhancing the reliability of out-of-distribution image detection in neural networks,” in *6th International Conference on Learning Representations, Vancouver, BC, Canada*, 2018.